Density dependence in demography and dispersal generates fluctuating invasion speeds

Sullivan et al. 10.1073/pnas.1618744114

Supporting Information (SI)

SI Table.

Table S1. All model parameters, definitions and corresponding models.

Variable	**Meaning**
t	time
x, y	locations
$n_t(x)$	population density at location x and time t
Parameter	**Meaning**
a	Allee effect threshold
r	intrinsic growth rate (overcompensatory model)
λ	low-density per capita reproductive rate (propensity and distance models)
$\hat{n}$	dispersal density midpoint parameter (propensity and distance models)
p	fraction of offspring that disperse
p_0	minimum dispersal propensity (propensity model)
p_{max}	maximum dispersal propensity (propensity model)
α	propensity shape parameter (propensity model)
σ^2	variance of the dispersal kernel
σ_0^2	minimum dispersal variance (distance model)
σ_{max}^2	maximum dispersal variance (distance model)
β	distance shape parameter (distance model)
Function	**Meaning**
$k(x-y)$	dispersal kernel
$f(n_t(x))$	growth or offspring density

SI Figures.

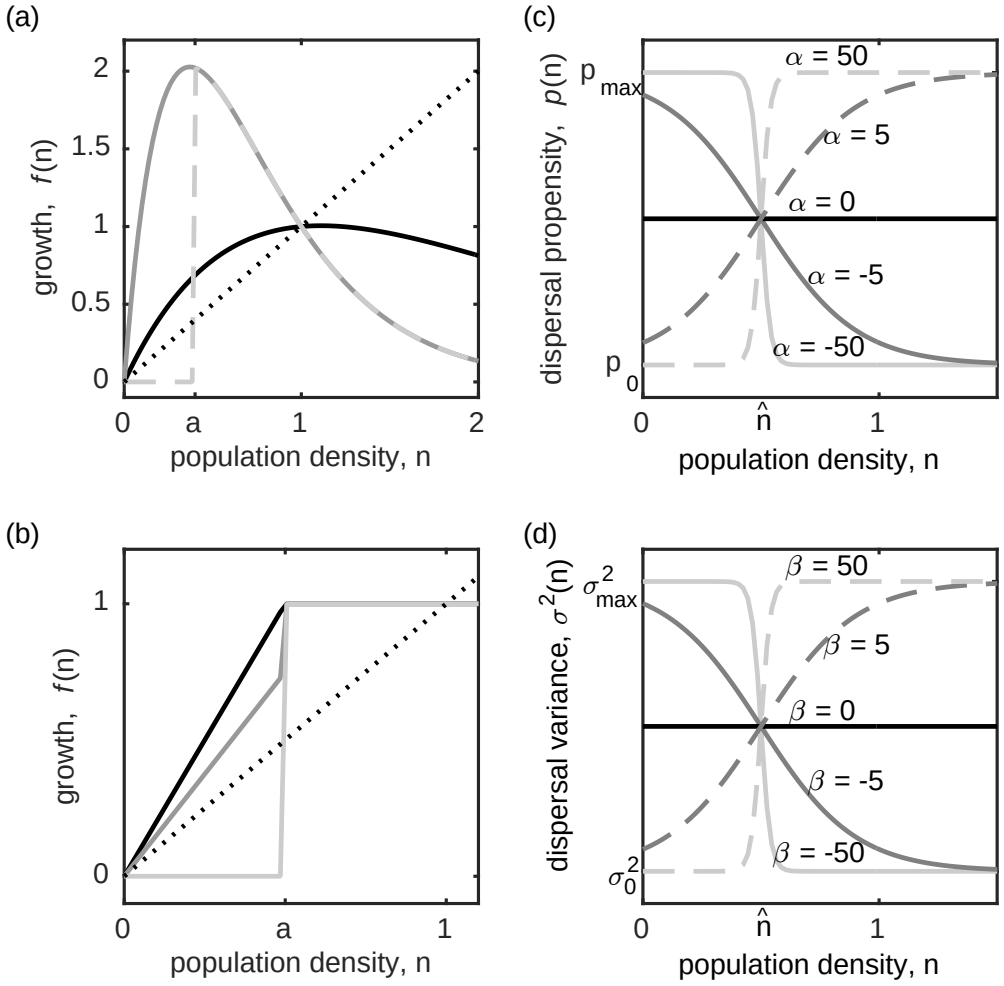

Fig. S1. Reproduction and dispersal functions used in the overcompensatory, propensity, and distance models (described in Materials and Methods). (a) The reproductive rate f(n) as given by Eq. 3 where $r = 0.9$ and $a = 0$ (same parameterization as Eq. 3 for Fig 1a, black), $r = 2.7$ and $a = 0$ (same parameterization as Eq. 3 for Fig 1b, dark gray solid), $r = 2.7$ and $a = 0.4$ (same parameterization as Eq. 3 for Fig 1c, light gray dashed). (b) The reproductive rate f(n) as given by Eq. 4 when $a = 0.5$ and $\lambda = 0$ (light gray), $\lambda = 1.5$ (dark gray), $\lambda = 2$ (black). Parameterization here is close to that of Fig 1d-f, except a is smaller here to more clearly visually demonstrate the differences between strong, weak and no Allee effects. (c) The propensity to disperse when altered by density dependence as given by Eq. 5 for different α. (d) The variance of the dispersal kernel when altered by density dependence Eq. 6 for different β values.

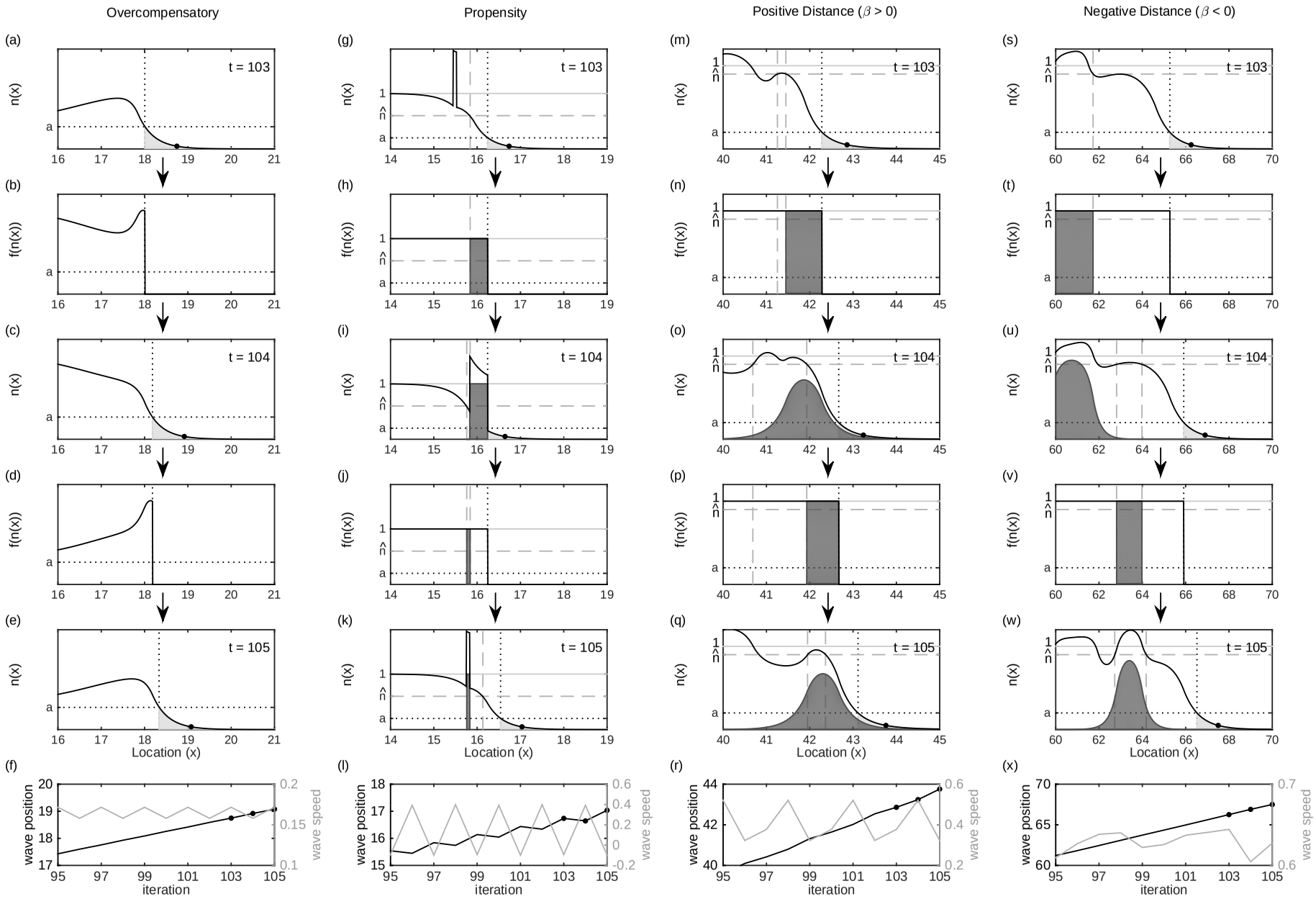

Fig. S2. Four examples of fluctuations in invasion speed. The top five rows show the population density before ($n(x)$) and after ($f(n(x))$) growth at sequential time steps, showing individuals that will not reproduce (light gray; $n < a$), those that do not disperse far (dark gray; $n > \hat{n}$ or $n < \hat{n}$), and the edge of the wave (solid point). The bottom row shows the wave position and speed over time. Parameter values and initial densities are the same as Fig. 2 except: (a-f) $r = 2.2$, $a = 0.4$, (g-l) $\hat{n} = 0.6$, $\alpha \to \infty$, (m-r) $\beta \to \infty$, (s-x) $\beta \to -\infty$.

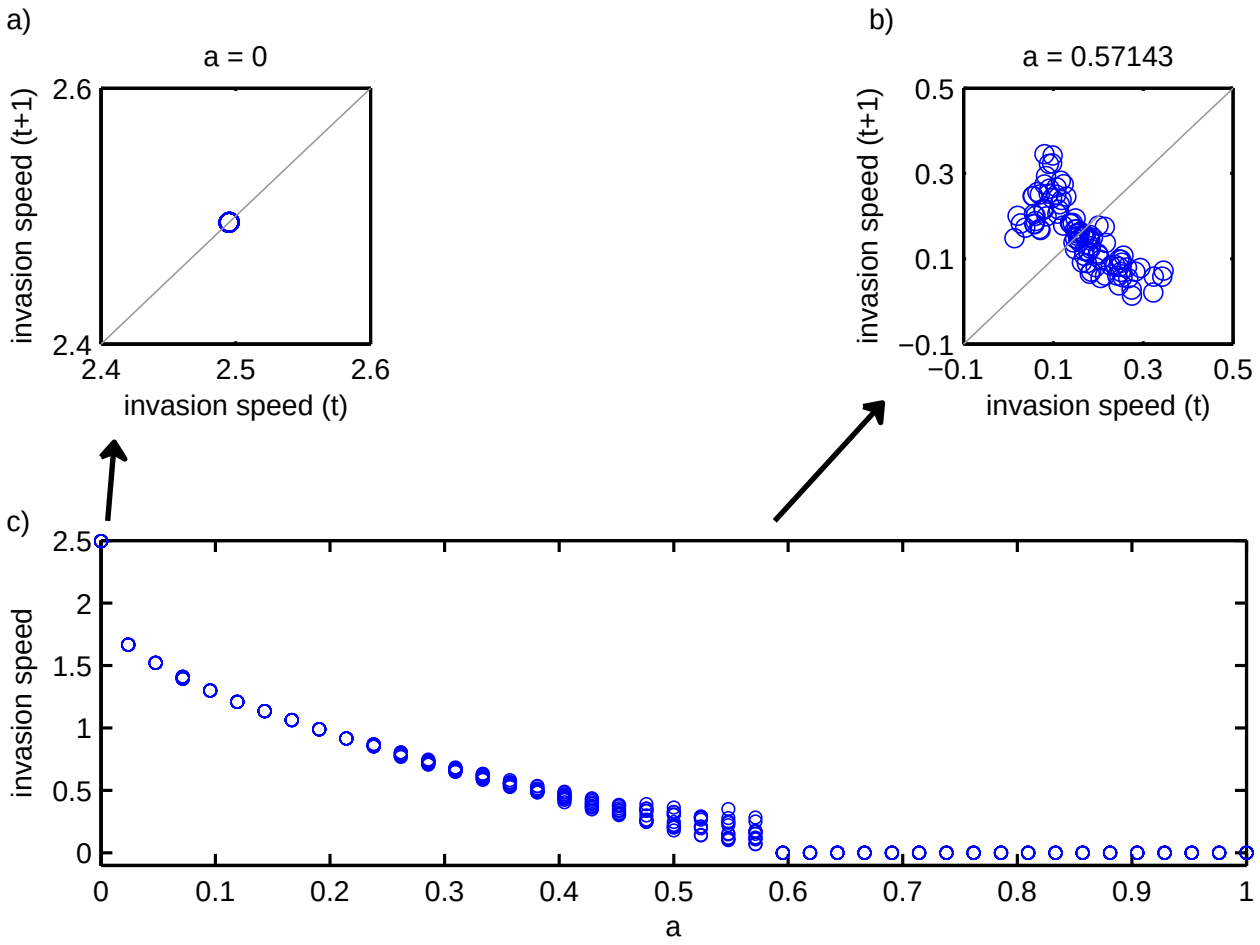

Fig. S3. The periodicity of the invasion speed through time for the overcompensatory model - Allee effects and overcompensation. In panels a-b, the wave position is plotted at time t vs time $t+1$. The wave speed ranges in periodicity across values of the Allee effect threshold a. At small values of a the invasion speed is constant (a), and at larger a values (b), the wave speed becomes chaotic until a becomes so large the population goes extinct. In panel (c), the range of invasion speeds represents the amplitude of fluctuations. At each plotted a value, the invasion speed for the previous 100 time steps are plotted. When points appear as hollow points, the same invasion speed is being plotted over itself many times. Here, $\sigma^2 = 0.25$.

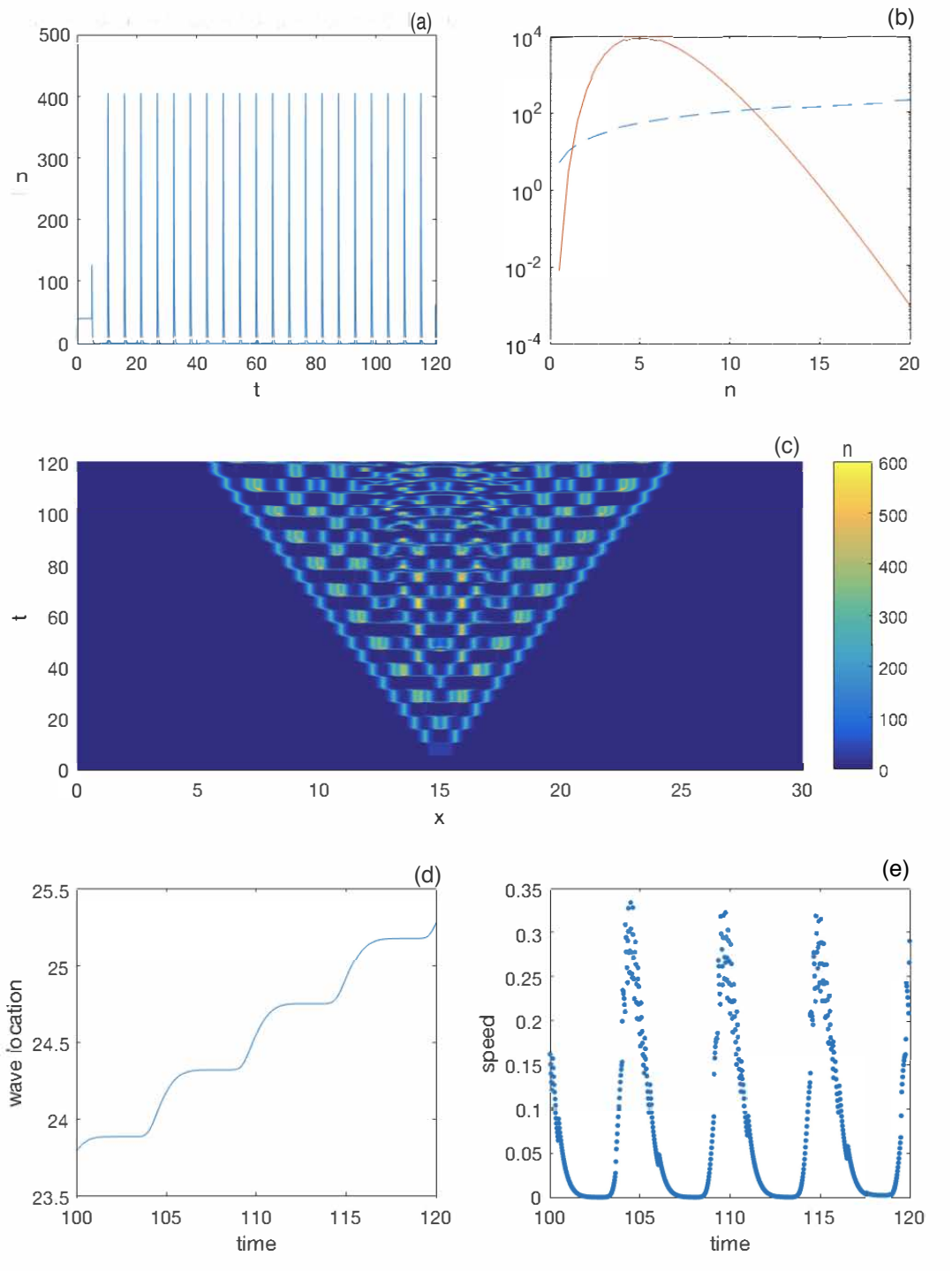

Fig. S4. Simulation of model (Eq. 2 from SI Appendix), with $a_1 = 20$, $a_2 = 2$, $a_3 = 10$, $\mu = 10$, $\tau = 5$, and $D = 0.1$. For these parameters the *undelayed* ordinary differential equation (Eq. 2 from SI Appendix with $D = 0$ and $\tau = 0$) exhibits a strong Allee effect, evident by comparing the mortality rate (dashed blue line) to the reproduction rate (solid red curve) in panel (b) (note the logarithmic scale). With delays, the model without movement (Eq. 2 from SI Appendix with $D = 0$) exhibits sharp generational cycles (a). The simulation of the partial functional differential equation (Eq. 2 from SI Appendix; initialized with $n = 2$ for $|x - 15| \leq 0.5$ and $0 \leq t \leq \tau$, and $n = 0$ otherwise) exhibits complex dynamics behind the invading fronts (c). These oscillations push the wave forward with a variable speed (d,e).

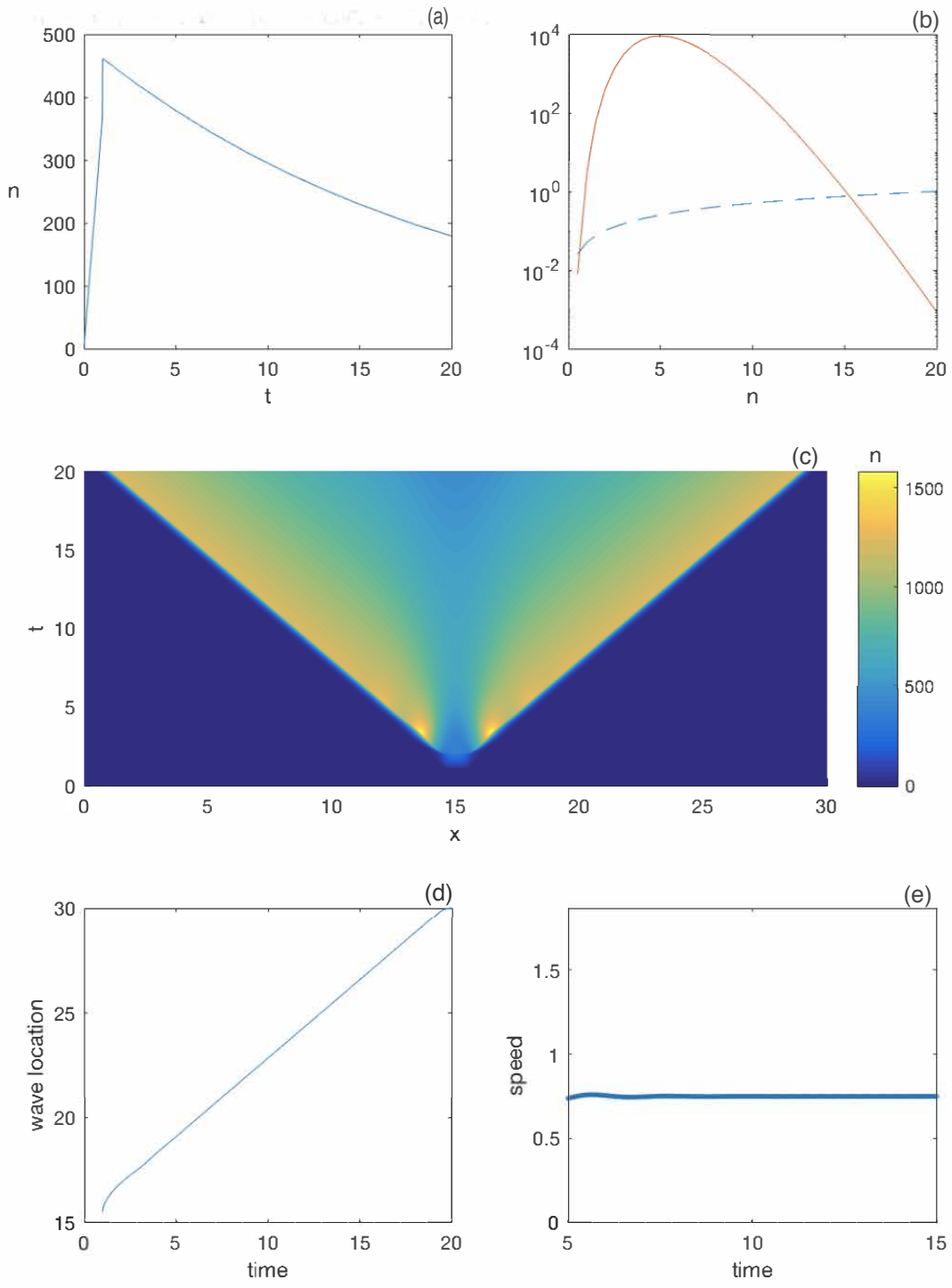

Fig. S5. Simulation of model (Eq. 2 from SI Appendix), with $a_1 = 20$, $a_2 = 2$, $a_3 = 10$, $\mu = 0.05$, $\tau = 1$, and $D = 0.1$. For these parameters the *undelayed* ordinary differential equation (Eq. 2 from SI Appendix with $D = 0$ and $\tau = 0$) exhibits a strong Allee effect, evident by comparing the mortality rate (dashed blue line) to the reproduction rate (solid red curve) in panel (b) (note the logarithmic scale). With delays, the model without movement (Eq. 2 from SI Appendix with $D = 0$) exhibits decay to a stable equilibrium (a). The simulation of the partial functional differential equation (Eq. 2 from SI Appendix; initialized with $n = 2$ for $|x - 15| \leq 0.5$ and $0 \leq t \leq \tau$, and $n = 0$ otherwise) exhibits simple dynamics behind the invading fronts (c). High population densities behind the wave front push the invasion forward with a constant speed (d,e).

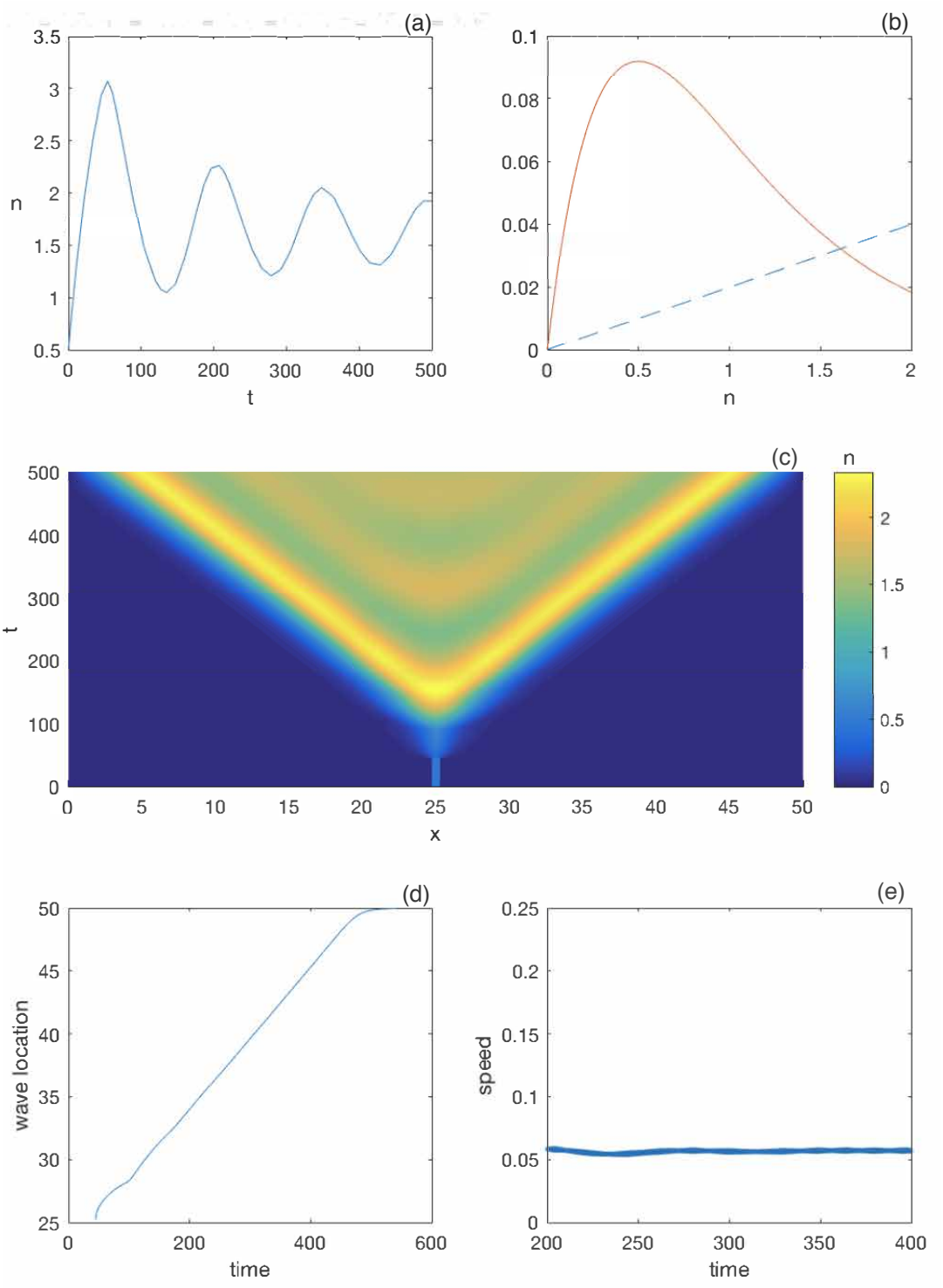

Fig. S6. Simulation of model (Eq. 2 from SI Appendix) with $a_1 = 0.5$, $a_2 = 2$, $a_3 = 1$, $\mu = 0.02$, $\tau = 45$, and $D = 0.05$. For these parameters the *undelayed* ordinary differential equation (Eq. 2 from SI Appendix with $D = 0$ and $\tau = 0$) does not exhibit any Allee effect, evident by comparing the mortality rate (dashed blue line) to the reproduction rate (solid red curve) in panel (b) (note the arithmetic scale). With delays, the model without movement (Eq. 2 from SI Appendix with $D = 0$) produces oscillations in population density (a). The simulation of the partial functional differential equation (Eq. 2 from SI Appendix; initialized with $n = 0.5$ for $|x - 25| \leq 0.5$ and $0 \leq t \leq \tau$, and $n = 0$ otherwise) exhibits oscillatory dynamics behind the invading fronts (c); however, the wave is "pulled" by growth at low densities, so a constant invasion speed is achieved despite the fluctuations at high densities (d,e).

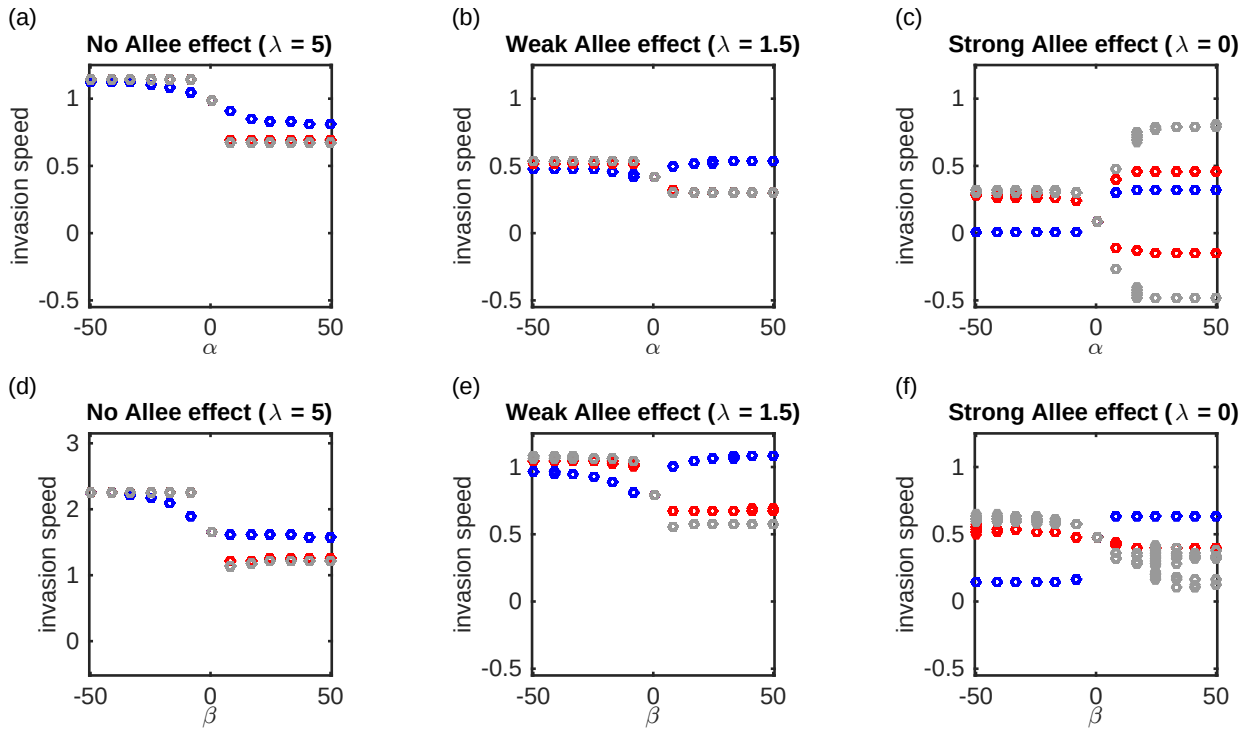

Fig. S7. Bifurcation diagram indicating fluctuations in invasion speed across a range of Allee effect strength for the propensity Model – when density dependence alters dispersal propensity (a-c), and the distance model – when density dependence alters dispersal distance (d-f). Here, we also show a range of dispersal thresholds ($\hat{n}$) relative to Allee effect threshold used for these models in the text ($a = 0.2$), including $\hat{n} = 0.1 < a$ (blue circles), $\hat{n} = 0.7 > a$ (red circles), and $\hat{n} = 0.9 >> a$ (gray circles). All other parameters are the same as Fig. 2. Fluctuations in invasion speed only occur when Allee effects are strong, when the dispersal threshold is high, and when $\alpha > 0$ (propensity model (a-c)) or across a range of positive and negative $\beta's$ (distance model (d-f)).

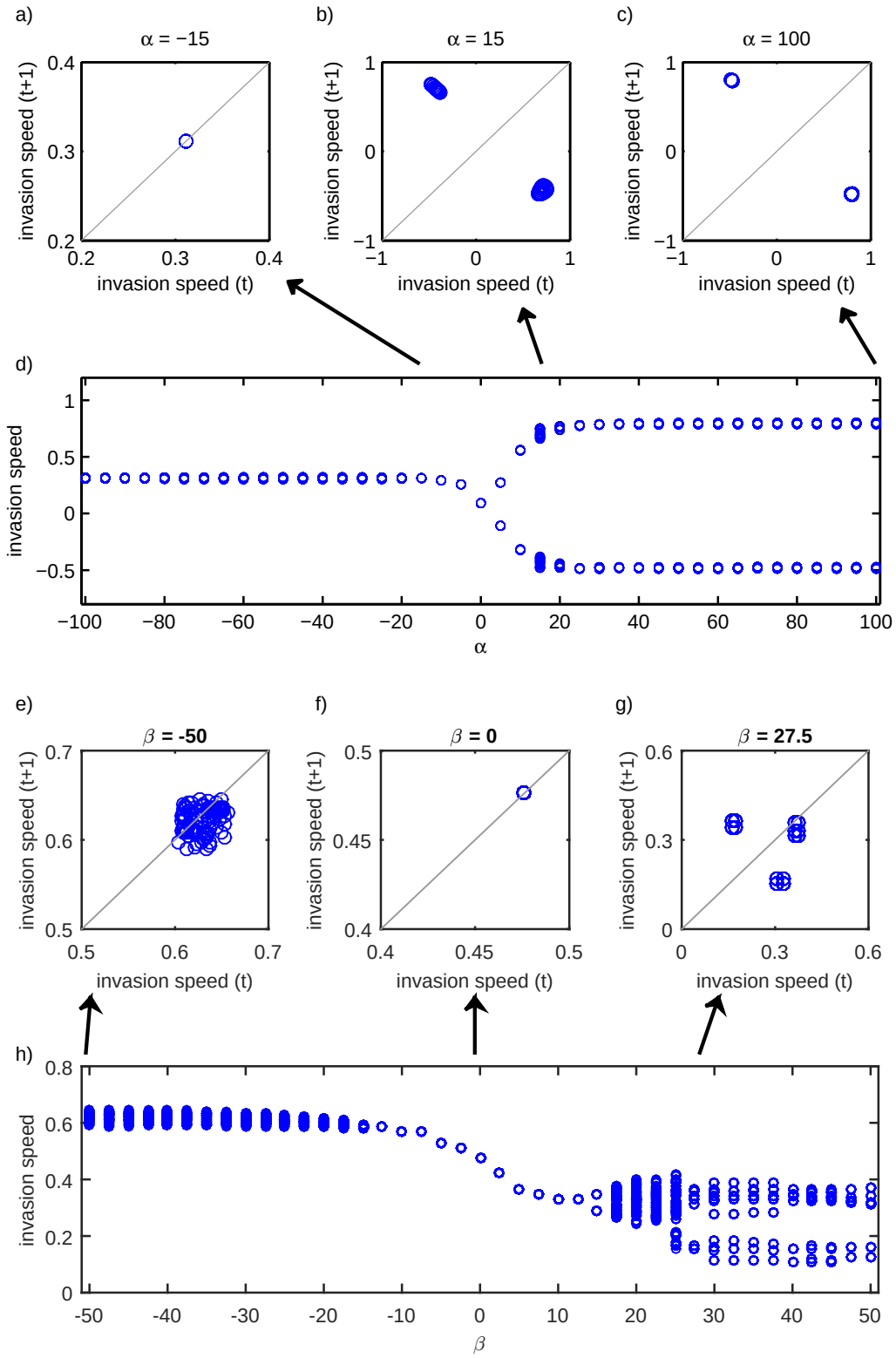

Fig. S8. The periodicity of the invasion speed through time for the propensity model (Allee effects and density-dependent dispersal propensity; a-d) and distance model (Allee effects and density-dependent dispersal *distance*; e-h). In panels a-c and e-g, the wave position is plotted at time t vs time $t+1$. In panels d and h, the range of invasion speeds represents the amplitude of fluctuations. For each parameter value, the invasion speed for the previous 100 time steps are plotted. When points appear as hollow points, the same invasion speed is being plotted over itself many times. For the propensity Model, when fluctuating, the wave speed is nearly always periodic across values of the Allee effect threshold a. At small values of α the invasion speed is constant (a), at small positive α the invasion speed fluctuates in a quasi-periodic fashion (b), and most positive α values, for example $\alpha = 100$ (c), the wave speed is periodic. Here, $\hat{n} = 0.9$, $\lambda = 0$, $\sigma^2 = 0.25$, $p_0 = 0.05$, $p_{max} = 1$, and $a = 0.2$. For the distance model, we demonstrate that the invasion speed appears to be more chaotic for some negative values of the density-dependent dispersal threshold (β) (e), is constant for some values of β (f), and has a quasi-periodic attractor for some positive values of β (g). Here, $\hat{n} = 0.9$, $\lambda = 0$, $\sigma_0^2 = 0.05$, $\sigma_{max}^2 = 1$, and $a = 0.2$.

SI Appendix.

Here we construct a continuous-time model that we conjecture produces variable-speed invasions. We begin with a modification of a delay-differential equation model used by Gurney et al. [1] to study the dynamics of "Nicholson's blowflies:"

$$\frac{dn}{dt} = -\mu n + a_1 n(t-\tau)\, e^{-a_2 n(t-\tau)}. \quad [1]$$

In this model, n is the population size of mature animals, and τ is the maturation time. The change in the adult population size is due to constant per captia mortality (at rate μ) and recruitment of juveniles, born τ time units ago, into the adult class. The per captia birth rate at low density (a_1) is reduced (exponentially at the rate a_2) at larger population densities. This model produces large swings in adult population size when the maturation time is sufficiently large [1].

We modify the model (1) to include the potential for a strong Allee effect (when the parameter $a_3 > 1$) and to include the random movement of adults via diffusion:

$$\frac{\partial n}{\partial t} = -\mu n(x,t) + a_1[n(x,t-\tau)]^{a_3}\, e^{-a_2\, n(x,t-\tau)} + D\frac{\partial^2 n(x,t)}{\partial x^2}. \quad [2]$$

Immature individuals are assumed to be sedentary.

The special case of model (2) with $a_3 = 1$ (without Allee effects) has been thoroughly studied (see, e.g., Lin et al. [2] and Solar and Trofimchuk [3] and references therein). The dynamics of this model in this case can be quite complex behind the leading invasion front, but, for biologically realistic initial conditions solutions, solutions exhibit an asymptotically constant spreading speed.

Much less is know about the dynamics of equation (2) when $a_3 > 1$, but the model would seem to have the features necessary to generate variable invasion speed. Density-dependent reproduction, along with the maturation time delay, induce population fluctuations at high density, and the Allee effect should generate a pushed wave. Our numerical simulations suggest that this is indeed the case (Fig. S4). When, in contrast, the population dynamics converge to an equilibrium point behind the invasion front, the invasion speed is eventually constant, even in the presence of an Allee effect (Fig. S5). In the absence of Allee effects ($a_3 = 1$), simulations of the model (2) produce constant speed invasions (Fig. S6), even if there are oscillatory dynamics behind the front, in agreement with prior theory.

1. Gurney, W.S.C., Blythe, S. P. and Nisbet, R. M. 1980. Nicholson's blowflies revisited. *Nature* **287**:17–21.
2. Lin, C-K., Lin, C-T, Lin, Y, and Mei, M. 2014. Exponential stability of nonmonotone traveling waves for Nicholson's blowflies equation. *SIAM Journal on Mathematical Analysis* **46**:1053–1084.
3. Solar, A. and Trofimchuk, S. 2015. Asymptotic convergence to pushed wavefronts in a monostable equation with delayed reaction. *Nonlinearity* **28**:2027–2052.